Available online at www.sciencedirect.com
SCIENCE DIRECT®
Journal of the European Ceramic Society 25 (2005) 1835–1853
www.elsevier.com/locate/jeurceramsoc

Plasma-sprayed glass-ceramic coatings on ceramic tiles: microstructure, chemical resistance and mechanical properties

Giovanni Bolelli[a], Valeria Cannillo[a], Luca Lusvarghi[a,*], Tiziano Manfredini[a], Cristina Siligardi[a], Cecilia Bartuli[b], Alessio Loreto[b], Teodoro Valente[b]

[a] *Dipartimento di Ingegneria dei Materiali e dell'Ambiente, Università di Modena and Reggio Emilia, Via Vignolese, 905-41100, Modena, Italy*
[b] *Dipartimento di Ingegneria Chimica e dei Materiali, Università degli Studi di Roma "La Sapienza", Via Eudossiana, 18-00184, Rome, Italy*

Received 3 March 2004; received in revised form 3 June 2004; accepted 20 June 2004
Available online 27 August 2004

Abstract

This article reports the characterisation and optimisation of glass-ceramic coatings plasma-sprayed on traditional ceramic substrates, dealing with microstructures, chemical resistance, and superficial mechanical properties. A $CaO–ZrO_2–SiO_2$ (CZS) frit, capable of complete crystallization after proper thermal treatment, has been employed: due to its refractory nature, its firing temperature in a traditional process would be unbearable for common substrates. The frit was plasma-sprayed onto ceramic tiles and a post-process thermal treatment has been developed in order to sinter and crystallize the coating, employing much lower temperatures than a traditional ceramic firing cycle. The microstructure of both as-sprayed and treated coatings has been evaluated with SEM and EDS, acid resistance tests have been performed. Vickers microhardness, superficial fracture toughness, deep abrasion resistance, elastic modulus and coating adhesion have been evaluated. Unglazed stoneware and an industrial glaze were also tested for comparison and an experiment was made to produce a CZS-based glaze to ascertain the inadequacy of traditional firing. As-sprayed coatings have a typical plasma-spraying defective microstructure, but a thermal treatment with 30′ isotherm at 850 °C plus 15′ isotherm at 1050 °C allows good densification, excellent adhesion and complete crystallization, with formation of wollastonite-2M and many small $Ca_2ZrSi_4O_{12}$ grains. Thus, the coating outperforms stoneware by 50% in abrasion resistance, possessing higher fracture toughness, thanks to the continuous crack deflections due to the numerous crystals. Fracture toughness appears to be the property most correlated to abrasion resistance, because brittle fracture is the dominant abrasion mechanism. Hardness and elastic modulus reflect quite well the coating inner cohesion. Treated coatings porosity is lower than industrial glazes and stoneware.

Keywords: Plasma-spraying; Microstructure-final; Glass ceramics; Chemical properties; Wear resistance; Toughness and toughening; Tiles

1. Introduction

All traditional glazing techniques involve application of a slip on a green (single-firing) or on a fired body (double-firing) and the firing of the glaze + substrate system.[1] This implies two main drawbacks: the requirement of glazes with the same firing temperature and almost the same thermal expansion coefficient as the substrate. These requirements impose limits on glazes compositions, preventing the adoption of high mechanical properties systems: in fact, common glazes have poorer superficial mechanical properties than unglazed porcelanized stoneware. In plasma spraying, instead, the substrate is only moderately pre-heated, and, should a post-process thermal treatment be needed, the temperature would be significantly lower than that of traditional firing processes. So, the coating can have higher melting point than the substrate, and thermal incompatibility troubles are greatly lessened.

A plasma torch consists of a tungsten cathode, a water-cooled copper anode with a central nozzle, and a gas feeding system; an arc is struck between the cathode and the

* Corresponding author. Tel.: +39 05 92056206; fax: +39 05 92056243.
E-mail address: lucalusv@unimore.it (L. Lusvarghi).

0955-2219/$ – see front matter © 2004 Elsevier Ltd. All rights reserved.
doi:10.1016/j.jeurceramsoc.2004.06.018

anode, across the gas flux, so that ionization of atoms and molecules transform the gas into a hot (up to 15,000 K) and high-velocity plasma. The coating material, in powder, is radially fed into the plasma flux just outside the nozzle exit: the particles are therefore dragged and heated by the plasma itself, so that they melt and accelerate towards the substrate.[2,3] The melted droplets impact on the substrate, flattening and solidifying in a few microseconds, assuming a typical lamellar (or splat-like) morphology. Every splat develops high tensile stresses after solidification because of its rapid cooling. In brittle materials, these stresses can only be relaxed through cracking:[4] therefore, the coating is quite defective because of intrasplat and intersplat microcracks, and also because of some pores;[5] hence, several sealing procedures have been developed.[6] Optimization of spraying parameters is possible only for a narrow particle diameters range,[7] but common granulometric distributions are generally larger. Pores and defects reduce the coating cohesion, and, therefore, enable abrasion through splats removal.[8–10] Microstructural modifications induced by post-process thermal treatments change the coating behaviour, so that its properties can be optimized. Since toughness can be expected to be the most important parameter in abrasion resistance of ceramic substrates and coatings, microstructural optimization must be aimed at the highest possible toughening: in general, glass-ceramic systems, where crystalline phases deviate the crack propagation path, show higher toughness than glasses.[11]

Elastic modulus is another interesting coating property, because it is directly correlated to the coating cohesion: plasma-sprayed coatings tend to give up at splat boundaries, behaving non-linearly and showing lower stiffness than corresponding bulk materials.[12] Cohesion improvement will be highlighted by an increasing elastic modulus of the coating. Due to the high temperature in the plasma, this technique is particularly fit for spraying ceramics, however, it has seldom been tested with glasses.[13–19]

2. Materials and characterisations

The employed frit belongs to the CZS system, and it is expressly designed for devetrification;[20] its nominal composition is listed in Table 1.

The spray powder has been produced by milling the frit with a fast planetary-moving mill, loading porcelain jars with frit and sintered alumina balls, in order to simulate the conventional ceramic milling process.

The milled powders have been subjected to chemical analysis to verify the actual composition (ICP-Atomic Emission Spectrometry, Liberty 200, Varian), differential thermal analysis to check transformation temperatures, like T_g and crystallization temperature (DSC 404, Netzsch, 20 °C/min heating), granulometric analysis (Particle Sizer Analysette 22, Fritsch), X-rays diffractometry (PW 3710, Philips, Cu Kα radiation), scanning electron microscopy (XL30, Philips). A dilatometric test has also been performed on a bulk sample, obtained by melting the frit and casting a glass bar (DIL 404, Netzsch, 10 °C/min heating).

Table 1
Chemical compositions of employed frit

Frit name	SiO_2	Al_2O_3	CaO	ZrO_2	Others
CZS	52%	Traces	31%	16.5%	Traces

Table 2
Plasma torch operating parameters

Torch type	F4-MB, nozzle internal diameter: 6 mm
Power	600 A × 72 V = 43.20 kW
Spraying distance	115 mm
Number of passes	Three pre-heating; 27 spraying
Powder injection system	Carrier gas: Ar, 3 slpm Injector axial distance from torch exit: 6 mm Injector radial distance from torch axis: 7 mm Injector internal diameter: 1.5 mm
Plasma gas composition and flow	Ar 50 slpm; H_2 14 slpm
Cooling system	Cooling gas: Ar, pressure 7 bar, flow not measured Nozzles: 2 nozzles, internal diameter: 4 mm
Substrate temperature during deposition	80–140 °C

Spray runs have been performed using a PT F4-MB plasma torch mounted in a Controlled Atmosphere Plasma-Spraying plant at Centro Sviluppo Materiali s.p.a., Castel Romano, Italy, co-shared with the University of La Sapienza (Roma):[19] following preliminary tests with different operation modes (APS, CAPS, HPPS), all depositions were performed in APS mode, using operating parameters listed in Table 2. The substrates were porcelanized stoneware and porous wall tile bodies, cut into 6 cm × 6 cm small tiles. The substrates thermal expansion coefficients were determined through dilatometry (30 °C/min heating). Substrates were grit-blasted at C.S.M. using a vacuum-operated Norblast blasting machine with hand-held blasting gun (internal diameter: 8 mm), the blasting distance (manually controlled by the operator) is about 100 mm and the blasting time is about 10 s, 20 grit angular alumina particles (Sulzer-Metco Metcolite-C) were employed. Grit-blasted surfaces were observed through SEM as well.

Thermal treatments have been performed according to the following schedule:

1. Single isotherm treatments: 15 °C/min heating to 1000 °C, 30 or 120 min isotherm at 1000 °C, slow cooling. These treatments are hereafter indicated as 1–30 or 1–120, respectively;
2. Double isotherm treatments: 15 °C/min heating to 850 °C, 30 min isotherm, 15 °C/min heating to 950 °C, 30 min or

60 min isotherm, slow cooling. These treatments are hereafter indicated as 9–30 or 9–60, respectively;
3. Double isotherm treatments: 15 °C/min heating to 850 °C, 30 min isotherm, 15 °C/min heating to 1050 °C, 15 min or 30 min isotherm, slow cooling. These treatments are hereafter referred to as 10–30 or 10–15, respectively.

The microstructural characterisation of as-sprayed and treated coatings has been performed on unpolished (as-sprayed) and polished surfaces, and on cross-sections. Samples were polished using 800 and 1000 grit SiC paper and 6 μm, 3 μm, and 0.5 μm alumina pastes, with 30 N load applied for 2 min for each paper and paste. Cross-sectional samples were cold-mounted in resin before polishing. Scanning electron microscopy was carried out together with a qualitative local chemical analysis through energy dispersive spectrometry. X-ray diffractometry was also performed to identify crystalline phases. To test acid resistance, the surface of the coating was left in contact with an 18% HCl solution for 4 days, then washed with water, optically inspected, and eventually treated with an organic dye (10% methylene blue aqueous solution) to highlight the possible increase in superficial porosity due to the chemical attack. The dye was washed away with water and then with a mild neutral detergent for glasses. The samples were also observed with SEM to look for microstructural details of the chemical attack.

For comparative purposes, the same morphological and chemical tests were also performed on commercial porcelanized stoneware and on an industrial high-quality glaze, fired both at 1200 °C for 45 min (stoneware-like firing cycle) and at 1130 °C for 40 min (single firing-like cycle) in an industrial fast kiln. The glaze compound contains a $CaO–Al_2O_3–SiO_2$ frit, sodium feldspar and quartz; the exact percentages have not been indicated as it is a proprietary formulation. The glaze is hereafter referred to as CAS glaze. Rugosimetry was performed on porous bodies, stoneware, and grit-blasted stoneware surface, using a Talysurf Plus rugosimeter from Taylor Hobson; six measurements were performed in each case (three parallel to one side of the tile, three parallel to the other), a measuring length of 15 mm with a cut-off length of 0.8 mm were employed in each case.

Furthermore, to confirm the unsuitability of conventional glazing techniques for the application of CZS, an attempt was made to produce and characterise a glaze containing as much CZS as possible, firing it at 1130 °C for 40 min and at 1200 °C for 45 min in an industrial fast kiln; the composition is listed in Table 3.

Table 3
Composition of a CZS-containing experimental glaze

Raw material	Quantity (%)
CZS frit	40
Sodium feldspar	53
Li-containing frit (very low T_g)	2
Dolomite	2.8
Kaolin	1.9
CMC	0.3

Glazes were applied, with laboratory instruments, both by aerography and by casting (standard laboratory technique to simulate the industrial "bell" application), trying to obtain the same thickness in both cases (several aerograph passes).

Mechanical characterization tests were performed on as-sprayed and double isotherm-treated coatings, on porcelanized stoneware and on CAS and CZS glazes. Moreover, a disk of bulk CZS glass was produced by melting the milled frit at 1550 °C in a muffle kiln, casting it in a disk-like cordierite crucible, annealing it at 820 °C (slightly above glass transition temperature) for 6 h to relieve residual stresses, then grinding it with 60-grit diamond abrasive paper to improve its discoid shape. This sample was mechanically characterized, then further annealed at 1050 °C for 1 h to induce crystallization and the subsequent glass-ceramic was also characterized. Vickers microhardness, elastic modulus, fracture toughness, deep abrasion resistance were measured.

Vickers microhardness (Remet HX-1000 Vickers microindenter) was measured both on polished surface and on polished cross-sections of the coatings, since it was reported that plasma-sprayed coatings sometimes show anisotropic behaviour;[21] for the other samples, only the cross-section was tested. To avoid indentation size effect,[22] in all cases the highest possible indentation load which did not cause cracking was adopted. Twenty indentations were performed for each measurement.

The elastic modulus of the coatings was measured using a 4-points bending test (4 p.b., Zwick/Roell Z010 testing machine, strain gauges on both sides of the sample), both with the coating in traction and in compression. The measurement was performed on as-sprayed coatings and on 10–30 treated coatings, cutting beam-like samples (length ≈ 60 mm, height and width ≈ 8 mm). The elastic modulus of bulk CZS glass, instead, was determined by a non-destructive technique based on the propagation of elastic waves across suitably supported samples: the resonance frequency of the elastic wave is determined with a microphone, and, from that, the elastic modulus and Poisson's ratio are found. To asses the comparability of these two techniques, stoneware elastic modulus has been determined in both ways.

Fracture toughness was measured through Vickers indentation technique: using high indentation loads, cracks propagate from the indent tips. Following indications given in literature,[23,24] the Lankford formula has been chosen for this research:

$$K_{Ic} = 0.0363\left(\frac{E}{H_V}\right)^{2/5}\frac{P}{a^{1.5}}\left(\frac{a}{c}\right)^{1.56}$$

where K_{Ic} = fracture toughness, in $N/\mu m^{3/2}$ ($1\ MPa \times m^{1/2} = 10^{-3}\ N/\mu m^{3/2}$); E = elastic modulus of the coating material in GPa; H_v = Vickers microhardness of the coating, expresses in GPa ($1\ kg/mm^2 = 9.81 \times 10^{-3}$ GPa); P = indentation load in N (1 kg = 9.81 N); a = indent average half-diagonal (μm); c = crack length, measured from the indent centre (μm).

Indentations were performed on the polished surface of all sprayed and treated coatings, bulk CZS glass and stoneware. Indentation time was 15 s in all cases. At least 10 indentations were performed for each measurement. Indent diagonals and cracks were measured through SEM images.

Deep abrasion resistance (Ceramic Instruments AP/87 abrasimeter) has been determined on all coatings, glazes and stoneware, through a three-body abrasion test. A flux of alumina particles (FEPA 80: mean diameter around 180 μm) falls tangentially to a rotating steel disk, pressed by a fixed load against the tested surface.

For an accurate trace length reading, the highest number of disk revolutions should be made. Since coatings with different thickness allow a different number of disk revolutions before the substrate is uncovered, in order to make the measurements comparable, the abraded volume is normalized by the overall distance L (in m) covered by the disk in its N revolutions, which is equal to $L = 2\pi dN$. Thus, the measurement is expressed as normalized volume $V_n = V/L$ (in mm^3/m).

Abrasion traces were also observed through scanning electron microscope (XL30, Philips) to identify abrasion mechanisms.

Adhesion of 10–30 CZS coatings on stoneware substrate has been evaluated with a tensile test: two steel plates (50 mm × 50 mm × 15 mm) with a central threaded hole are glued to the coating surface and the substrate base of a 50 mm × 50 mm sample tile using a high tensile strength epoxy glue (Plasmatex Klebbi, nominal tensile strength = 100 MPa), cured for 1 day at 90 °C; a threaded bar hold is threaded into each plate hole. The bar holds are sized in the tensile testing machine (Galdabini PM 60 universal testing machine) clamps, displaced at 5 mm/min.

3. Results and discussion

3.1. Microstructural characterization and chemical resistance

3.1.1. Powders characterization

The best ball milling results were achieved loading 1 l porcelain jars with 500 g of frit and 500 g of 25 mm diameter alumina balls, and sieving the powders between 45 μm and 75 μm. This process does not significantly pollute the frit, as the balls weight loss after each milling operation is lower than 0.1%. Fig. 1 indicates the granulometric distribution: the maximum of the distributive curve lies at around 40 μm, an optimal particle size for plasma-spraying, although the distribution is not narrow around this value. SEM micrographs (Fig. 2) indicate the particles have an irregular morphology, since mechanically crushed.

The actual composition is reported in Table 4, with oxides percentages ratios listed in Table 5. Slight experimental errors (probably calibration imperfections in the ICP instrument) make it difficult to obtain analyses where the sum of oxide percentages is 100%, notwithstanding

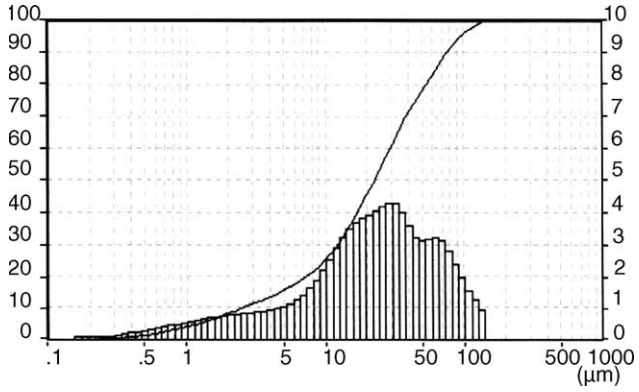

Fig. 1. Distributive and cumulative curve of CZS frit dry-milled and sieved between 45 μm and 75 μm.

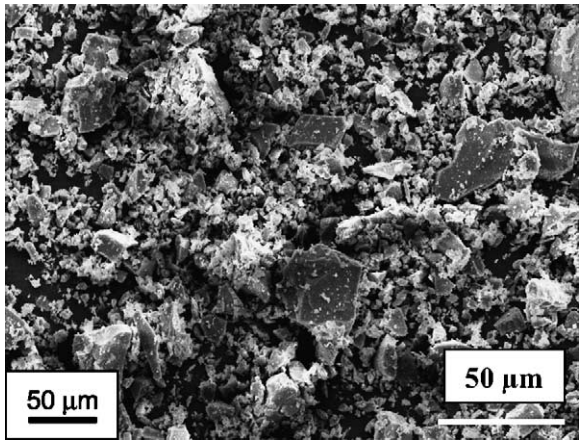

Fig. 2. SEM micrograph of milled CZS powder.

many attempts; no other oxides, however, are present in significant amount except those listed, as EDS analyses confirm.

The use of industrial raw materials in the frit production implies the addition of some impurities, the major difference between nominal and actual composition being the addition of alumina, which is due to the raw materials composition. However, the ratios between the main oxides are in good agreement with nominal values; the actual composition seems a little richer in ZrO_2.

Differential thermal analysis (Fig. 3) indicates that the frit has $T_g \approx 780$ °C and crystallizes at about 1050 °C, forming

Table 4
Actual composition of CZS dry-milled frit

Oxide	CaO	SiO_2	ZrO_2	Al_2O_3	K_2O	Na_2O	MgO	Total
Percentage	28.36	48.41	16.09	2.06	0.97	0.52	0.45	96.86

Table 5
Ratios between major oxides

Oxides ratio	CaO/ZrO_2	CaO/SiO_2	ZrO_2/SiO_2
Actual value	1.763	0.586	0.332
Nominal value	1.879	0.596	0.317

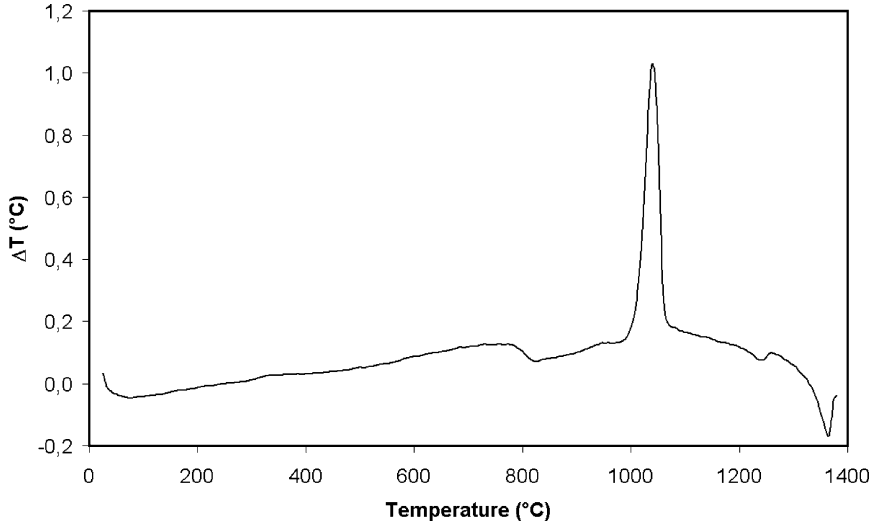

Fig. 3. Differential thermal analysis of CZS frit.

wollastonite-2M and $Ca_2ZrSi_4O_{12}$ as main phases, as already described by other authors.[20] Two endothermal peaks appear at 1240 °C and 1360 °C, probably due to phase transition (for instance wollastonite → pseudowollastonite) or melting of some phases.

Thermal expansion coefficient of CZS is:

$$\alpha = 74.8 \times 10^{-7}\,^{\circ}\mathrm{C}^{-1} \quad \text{for } 100\,^{\circ}\mathrm{C} < T < 500\,^{\circ}\mathrm{C}.$$

X-ray diffractometry indicates the presence of some unmelted zircon (JCPDS file 6–266), because of the frit production process.

3.1.2. Substrates characterisation

The thermal expansion coefficients of the substrates are:

porcelanized stoneware:	$\alpha = 84.9 \times 10^{-7}\,^{\circ}\mathrm{C}^{-1}$	for $50\,^{\circ}\mathrm{C} < T < 550\,^{\circ}\mathrm{C}$;
single-fired porous bodies	$\alpha = 79.4 \times 10^{-7}\,^{\circ}\mathrm{C}^{-1}$	for $110\,^{\circ}\mathrm{C} < T < 550\,^{\circ}\mathrm{C}$.

It is therefore obvious that pure CZS frit would not be applicable through traditional technologies: the firing temperature of CZS powder is intolerable for the substrate and huge dilatometric incompatibility would arise after firing.

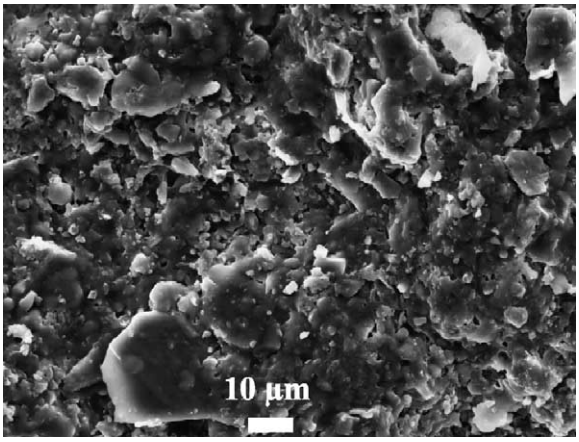

Fig. 5. Surface of porous wall tile body.

Stoneware has a quite irregular, low-porosity surface (Fig. 4A), characteristic of the pressing and sintering

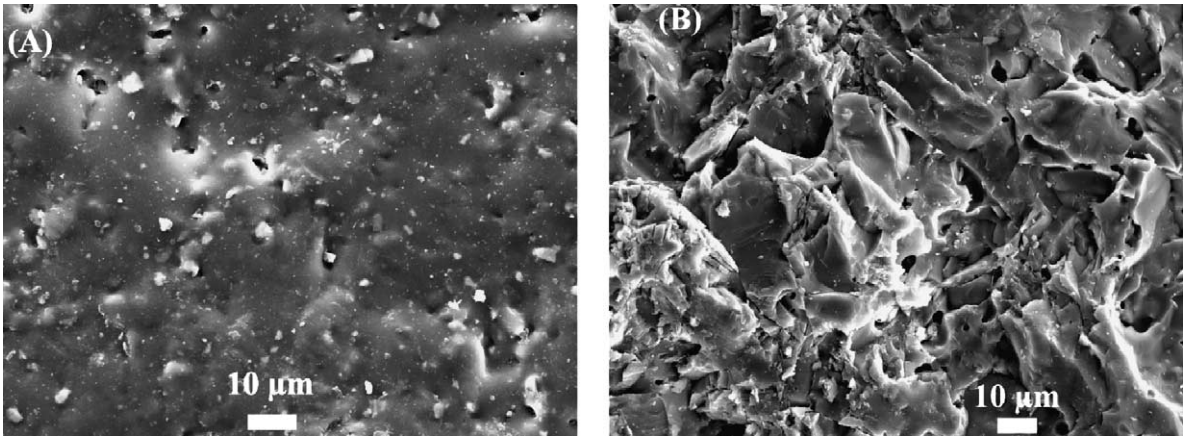

Fig. 4. SEM micrograph of stoneware surface before (A) and after grit-blasting (B).

Table 6
Results of roughness measurements

Material	$R_a \pm \Delta R_a$ (μm)	$R_y \pm \Delta R_y$ (μm)	$R_a \pm \Delta R_a$ (μm)
Porcelanized stoneware	2.42 ± 0.19	21.2 ± 4.04	16.6 ± 2.17
Grit-blasted porcelanized stoneware	5.96 ± 0.49	40.53 ± 6.49	30.07 ± 2.75
Porous wall tile body	6.58 ± 0.70	51.80 ± 5.42	37.56 ± 3.00
Grit-blasted porous wall tile body	8.47 ± 0.95	65.28 ± 6.29	44.74 ± 4.58

process: the surface is where sintering first takes place, furthermore, pressing compacts the surface more than the interior of a material. XRD indicates that such surface consists of a glass matrix (formed by melting the sodium feldspar at high temperature) containing quartz (whose primary function is to lower product cost), zircon (added in great quantity to whiten the tile), mullite (tough crystalline phase originated by kaolinite transformations during firing), and residual unmelted feldspars. The surface compactness and the presence of phases with good chemical stability make this product quite resistant to acid attack, as shown by the acid resistance test result: no visible effect is perceivable and a slightly more dyed zone is observed in the attacked region. Subsequent SEM analysis has not revealed an evident microstructural damage.

Porous wall-tile bodies have extremely high porosity and a very irregular surface (Fig. 5), which is fit to promote mechanical bonding of the coating. Because of the reactive consolidation mechanism, XRD reveals the presence of several crystalline phases: quartz, albite, anorthite, ghelenite, enstatite, wollastonite. Obviously, no chemical or mechanical tests were performed on such material, as they would be meaningless because of the high porosity (≈20%).

The irregularity of the surfaces of both substrates suggests that sand-blasting might be useless. Results from rugosimetric measurements are listed in Table 6.

Stoneware roughness is increased by grit-blasting, but it is quite rough anyway. The grit-blasted stoneware surface has undergone a severe damage by brittle fracture mechanism (Fig. 4B), which can likely interfere with an optimal coating adhesion (Fig. 6A). Porous bodies are already very rough, and sand-blasting only causes them severe damage (Fig. 6B). Thus, we can conclude that grit-blasting is to be avoided in further experiences, even if it produces slightly improved roughness homogeneity in porcelanized stoneware.

3.1.3. Glazes characterization

The following pictures (Fig. 7) represent the cross-sectional microstructure of the CAS glaze fired with both cycles (aerograph and casting deposition techniques do not significantly differ). Although the porosity is mostly closed in both cases, there are several large pores (≥50 μm), particularly after the 1130 °C firing cycle: the high viscosity of the CAS glass makes powders sintering very difficult. It is reasonable to expect that such pores reduce mechanical properties. XRD measurements on the 1130 °C fired sample indicate the presence of quartz, residual unmelted albite, and pseudowollastonite, originated by mild crystallization of the CAS frit. In the 1200 °C sample only quartz is present, because the temperature was high enough for albite to melt completely. The CAS frit composition equals the ternary $CaO–Al_2O_3–SiO_2$ eutectic at 1170 °C, therefore, firing at 1200 °C, the pseudowollastonite formed by the CAS frit melts. SEM–BSE micrographs particularly highlight the darker quartz grains: it can be noticed that the glaze looks like a composite system, with quartz grains acting as reinforcing particles.

The presence of some large pores reduces the chemical resistance of these glazes (Fig. 8): dye treatment highlights a clear colour change in the 1130 °C fired sample, which retains higher porosity and phases, like pseudowollastonite, which

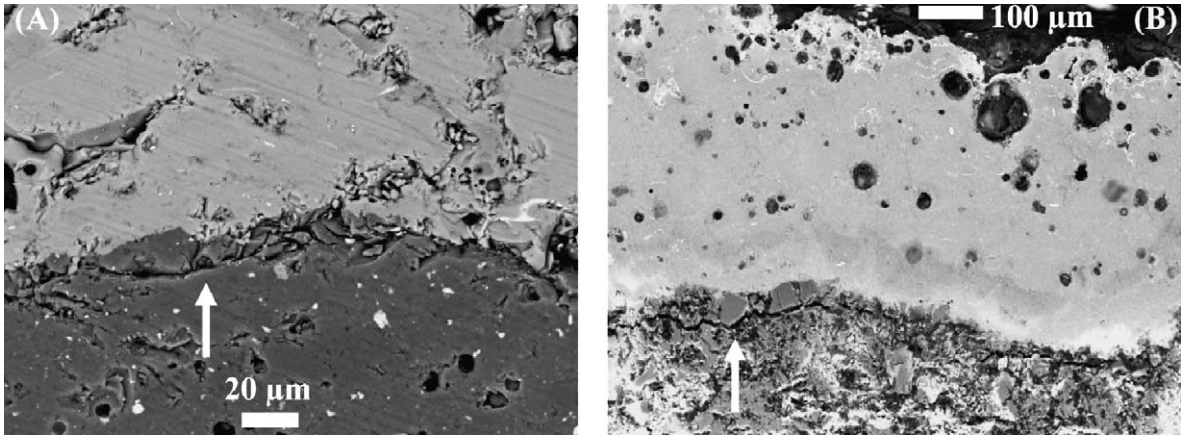

Fig. 6. Detail of sub-superficial grit-blasting damage in porcelanized stoneware (A) and large sub-superficial crack in porous wall tile body (B).

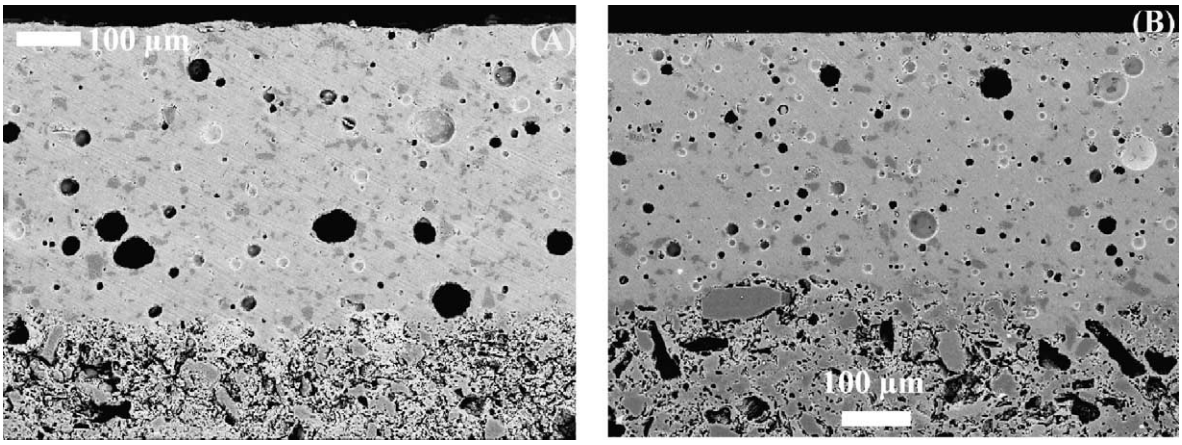

Fig. 7. Cross-section of CAS glaze fired fired at 1130 °C for 40 min (A) and at 1200 °C for 45 min (B).

do not have a remarkable chemical resistance. The 1200 °C fired sample, having lower porosity and no pseudowollastonite, appears to be more resistant.

The CZS-based experimental glazes, fired at both temperatures, are represented in Fig. 9A and B. The 1130 °C firing leaves a lot of open porosity, in fact the chemical resistance test cannot be performed on this glaze because all of the acid solution is absorbed. The 1200 °C firing does not leave open porosity, but there are a lot of pores larger than 50 μm: notwithstanding the formation of a lot of crystalline phases in the CZS frit, which could toughen the material, the excessive porosity is likely to lower significantly the mechanical properties. In the 1130 °C fired glaze, X-rays diffractometry indicates the presence of a significant amount of glassy phase together with crystalline phases: $Ca_2ZrSi_4O_{12}$ and wollastonite-2M, typical crystalline phases formed by the CZS frit, some zircon (deriving from the frit) and unmelted albite. The 1200 °C firing produces a more complete crystallization of the frit, therefore the relative amount of glassy phase (qualitatively evaluated from diffractograms) is lower; the main crystalline phase is with wollastonite-2M and zircon as secondary phases; all of the albite has been melted. The absence of open porosity, together with the more complete crystallization and the formation of more acid resistant species ($Ca_2ZrSi_4O_{12}$ at the expense of wollastonite), increase the chemical properties of this glaze: even after dye treatment, no changes were perceivable.

3.2. Plasma-sprayed coatings microstructures

3.2.1. As-sprayed coatings

Cross-sectional micrographs show that as-sprayed coatings have a very defective microstructure (Fig. 10A), typical of the plasma-spraying process: besides the presence of pores due to gas entrapment between splats, there are a few unmelted particles and, in particular, interlamellar and intralamellar microcracks, which reduce the coating cohesion.[8,9] Image analysis has indicated a porosity value around 15%. Notwithstanding this defectiveness, the interface with the substrate appears of good quality, as the coating follows all the substrate irregularities.

Since the CZS system is prone to devetrification, thermal cycling in the lower coating layers due to repeated torch runs can induce nucleation of crystalline phases. In the cross-

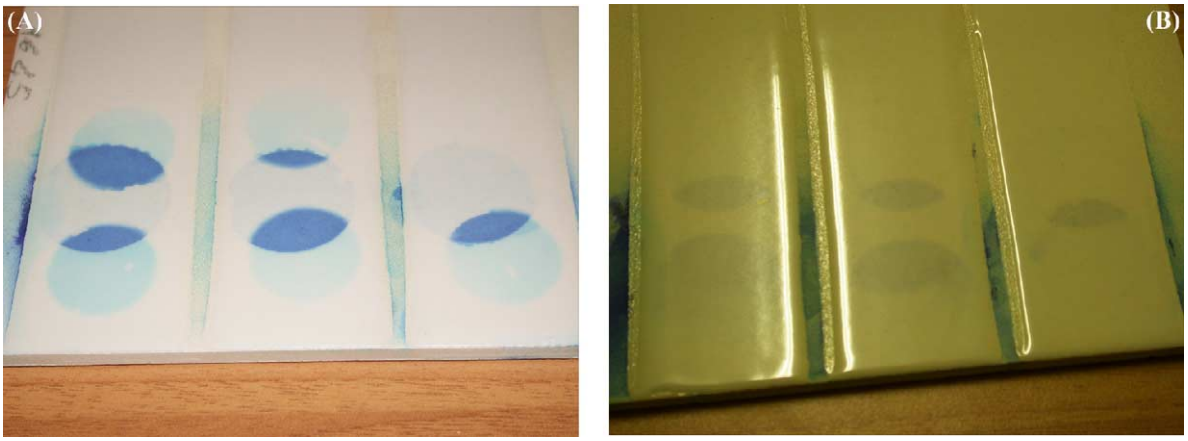

Fig. 8. Chemical resistance test on CAS glaze 1130 °C 40′ (A) and 1200 °C 45′ (B) glazes after dye treatment.

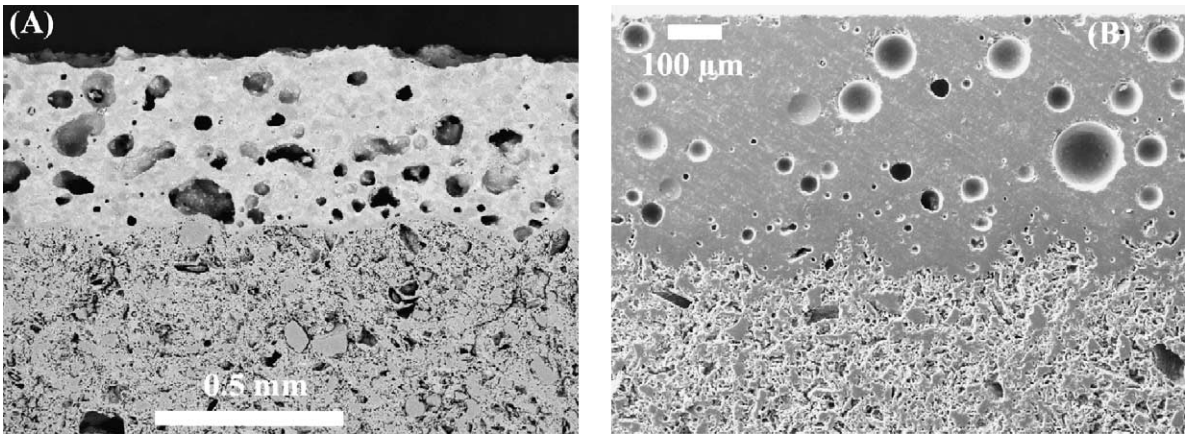

Fig. 9. Cross-section of CZS-based glaze fired at 1130 °C for 40 min (A) and at 1200 °C for 45 min (B).

section, especially in the lower layers, there are some small lamellar white grains: EDS qualitative chemical analyses shows these grains to be richer in Ca and Zr than the surrounding glass matrix, and XRD highlights the existence of a very little amount of $Ca_2ZrSi_4O_{12}$ inside a glassy matrix. Slight peaks of monoclinic zirconia are sometimes present in diffractograms: the plasma high temperature heats the residual unmelted zircon present in the powders, exceeding its dissociation temperature (around 1600 °C), so that it decomposes into SiO_2 (entering the glass matrix) and ZrO_2.

On the surface of the as-sprayed coating (Fig. 10B), the splats are clearly noticeable: there are disk-like splats, fingered splats, and also some larger, partially unmelted splats not completely flattened. Their presence, due to the larger powder particles, is one of the causes of the elevated observed porosity. The presence both of disk-like splats and fingered splats is due to the quite broad granulometric distribution: many studies[25–27] have shown that the splats morphology depends on the particles motion characteristics, but particles with different size are differently accelerated and heated by the plasma flux, developing different motion regimes.

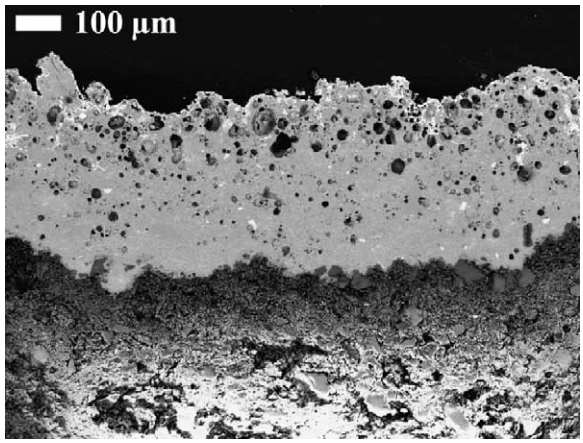

Fig. 11. Cross section of 1–120 CZS coating.

Chemical resistance tests cannot be performed with as-sprayed coatings on porous substrates, because the acid solution passes through the open porosity in the coating and is completely absorbed by the substrate itself. Performing

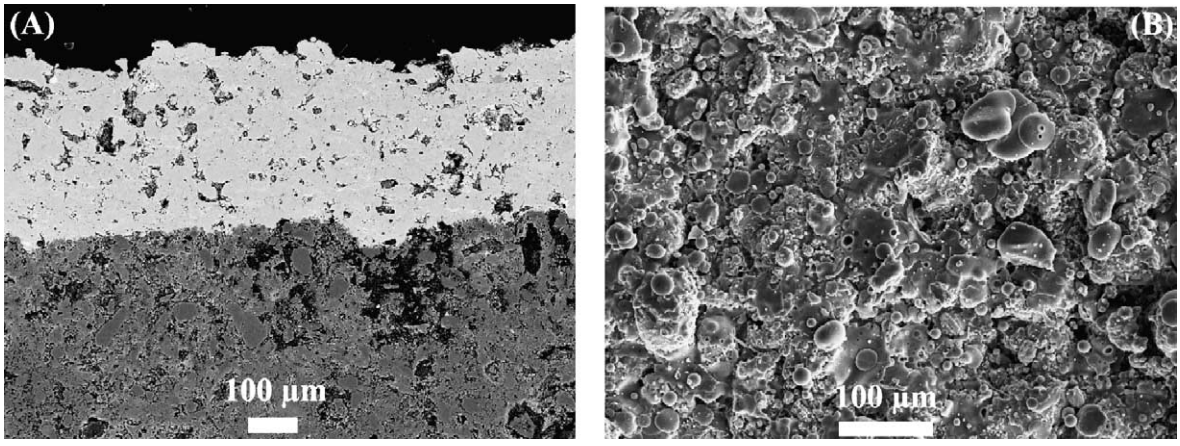

Fig. 10. Cross-section (A) and surface (B) of as-sprayed CZS coating on porous wall-tile body.

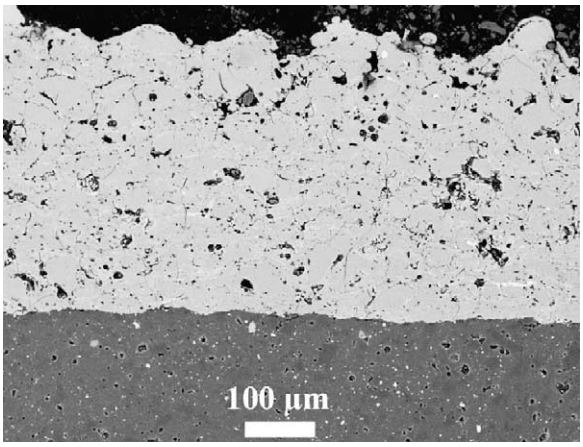

Fig. 12. Cross section of 850 °C 30′ annealed CZS coating on stoneware.

the test on coatings on stoneware substrates, the resistance appears to be quite low, because the pores produce a very high superficial area. Besides, the coatings are significantly stained by the dye, as it is absorbed by the pores and cannot be washed away any more. These results point out to the need for thermal treatments to sinter and crystallize the coating.

3.2.2. Single isotherm-treated coatings

In cross section (Fig. 11), both after the 30′ thermal treatment and after the 120′ one, we can notice a good sintering of the lower layers of the coating, while its surface retains an elevated porosity. During sintering, the air contained in the pores moves through the viscous glass up to the surface, but, since, with a single isotherm, crystallization and sintering are concurrent, the surface turns from a viscous glass into a crystalline solid before the air motion is complete. According to these results, single isotherm thermal treatments have been discarded and no other tests were performed on them.

3.2.3. Double isotherm-treated coatings

The first step at 850 °C enables sintering to begin without being immediately hindered by crystallization: after this step, the material is not completely sintered, but it can be seen (Fig. 12) that the overall porosity is reduced and somewhat modified in nature, as round pores appear, although some microcracks still remain. No crystallization has taken place in this step.

The second step at 950 °C, both for 30′ and 60′, enables optimal sintering but no significant crystallization (Figs. 13A and 14): the increased temperature reduces the glass phase viscosity, thus enhancing air release, but 950 °C is not enough to induce complete devetrification. The interface quality increases: wollastonite nucleates in the coating at the substrate interface, since the substrate decidedly lowers nucleation activation energy. Therefore, the adhesion is not only mechanical, but also chemical. The porosity is lower than all tested glazes, all pores are round in shape, few larger pores do not exceed 20 μm in diameter.

Chemical resistance has not been tested on this coating, since the goal was to obtain a toughened glass-ceramic: optimal sintering is not the only goal of thermal treatments.

Coatings 10–30 and 10–15 are, instead, completely crystalline: XRD indicates the presence of large amounts of monoclinic wollastonite (also referred to as −2M, JCPDS file 27–88) and $Ca_2ZrSi_4O_{12}$ (JCPDS file 39–194), with some larnite (β-Ca_2SiO_4, JCPDS file 33–302) and baghdadite ($Ca_3ZrSi_2O_9$, JCPDS file 39–195) too, and very few glass phase left (Fig. 14). Cross-sectional micrographs (Figs. 13B and 15) indicate, first of all, the presence of many interlaced dendrites in the matrix, which are identifiable as wollastonite through EDS analysis. Such a matrix is likely to be more tenacious than a glass matrix, since the dendrites interlacing hinders cracks propagation. Besides, numerous micrometric and sub-micrometric crystals (white in BSE imaging) of $Ca_2ZrSi_4O_{12}$ are present: in this way, the coating microstructure becomes similar to that of composite materials with particulate reinforcement, thus potentially enhancing mechanical properties. Porosity is low (between 4% and 6% from image analysis), with pores no larger than 20 μm (with few local exceptions), but it is slightly higher than the former case S (9–30; 9–60) because of small micrometric and

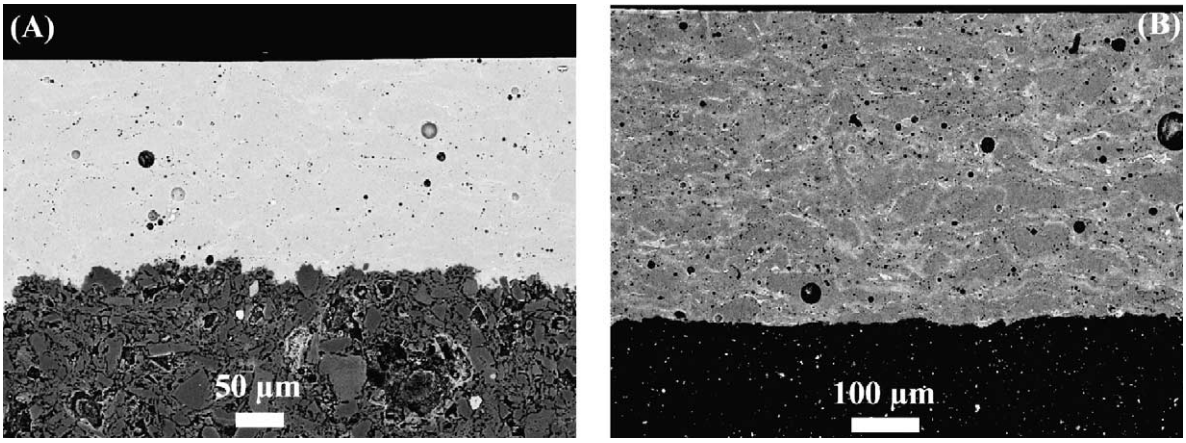

Fig. 13. Cross section of 9–30 CZS coating on porous wall tile body (A) and of 10–30 CZS coating on porcelanized stoneware (B).

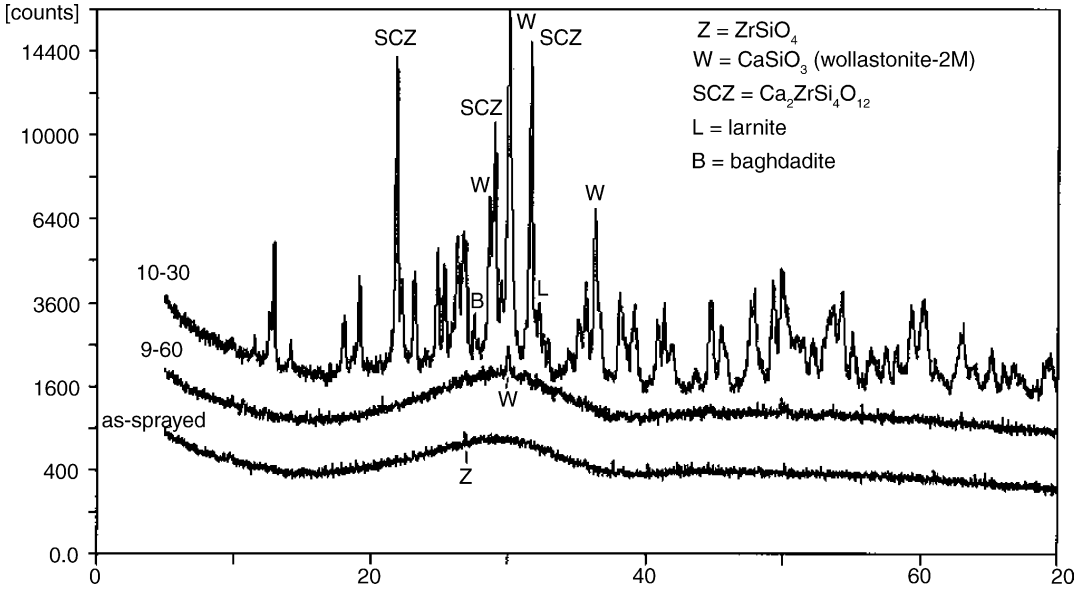

Fig. 14. XRD patterns of as-sprayed CZS coating (no grinding), 9–60 CZS coating (ground surface) and 10–30 CZS coating (ground surface).

sub-micrometric pores. The formation of crystals having a different specific volume than the glass can open some sub-micrometric pores, furthermore, crystallization hinders the prosecution of sintering after the first stage. Surface micrographs (Fig. 16) confirm these observations and underline that $Ca_2ZrSi_4O_{12}$ small crystals appear in clusters. Image analysis indicates that, in both 10–30 and 10–15 cases, the volume percentage of $Ca_2ZrSi_4O_{12}$ on the overall material present (excluding pores from the count) is around 15.5%. The difference between these coatings is not large, which indicates that the more time-saving 10–15 treatment is to be preferred for economical reasons. The only microstructural difference is the increased number of crystal grains (both wollastonite and $Ca_2ZrSi_4O_{12}$) and their reduced dimensions: toughening mechanisms theory suggests that the smaller and more numerous the toughening phases, the tougher the material, therefore we can expect that 10–15 coating will mechanically outperform 10–30.

Distinguishing larnite from wollastonite and baghdadite from $Ca_2ZrSi_4O_{12}$ by BSE imaging with qualitative EDS analysis is not possible, because of the small compositional difference.

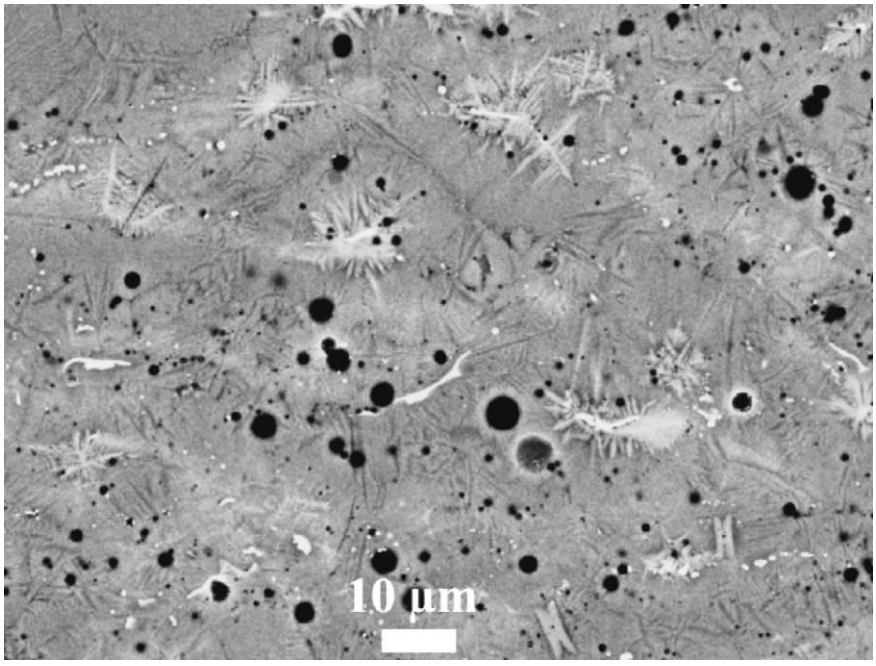

Fig. 15. Detail of cross-section of 10–30 CZS coating on porcelanized stoneware, showing extensive crystallization.

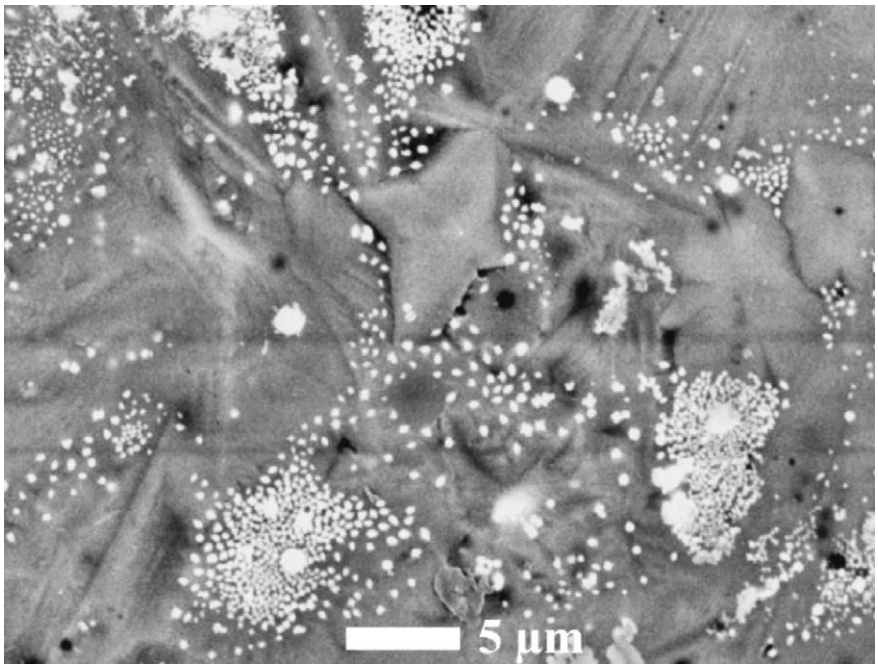

Fig. 16. Surface micrograph of 10–15 CZS coating.

Thermal expansion coefficients mismatch between the CZS crystallized coating and porcelanized stoneware would have caused the tile to be deformed if a traditional, high-temperature (≥1200 °C) firing cycle had been performed: at such temperatures, the crystalline phases of the coating are solid and cannot undergo significant viscous flow; instead, the glassy phases in stoneware have relatively low viscosity (their glassy transition temperature having been far exceeded), so that they accommodate the thermal expansion mismatch stresses through viscous flow, resulting in macroscopic tile deformation. In this case, the firing temperature is low enough for the glass phase in stoneware to retain high viscosity ($T_g \approx 820$ °C, dilatometric softening temperature >1050 °C, as determined through dilatometry), so that no deformation takes place: compressive stresses are therefore likely to develop in the coating, but the coating and the inter-

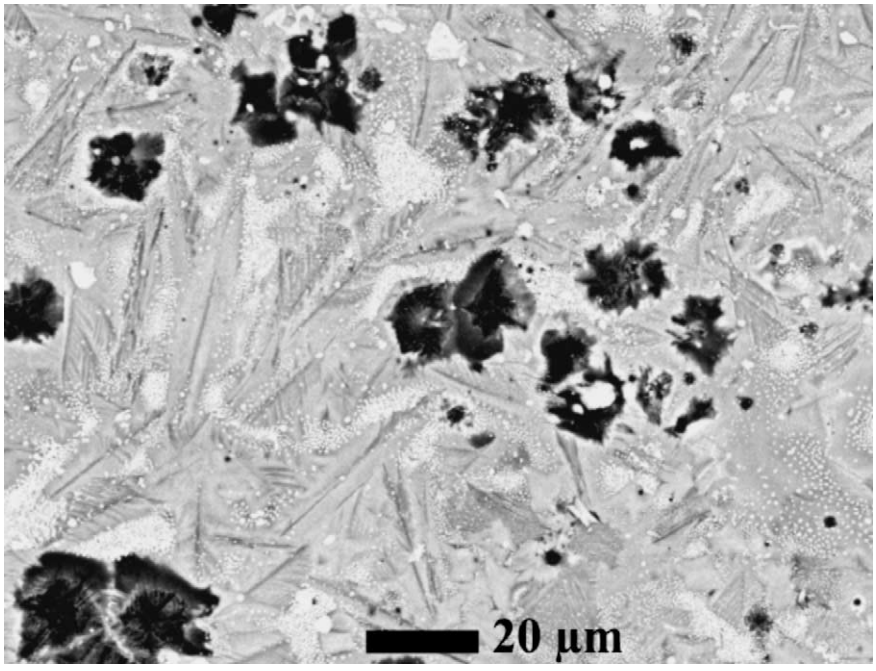

Fig. 17. Micrograph of the dye-treated zone at the border between attacked and unattacked area, showing selective attack on wollastonite.

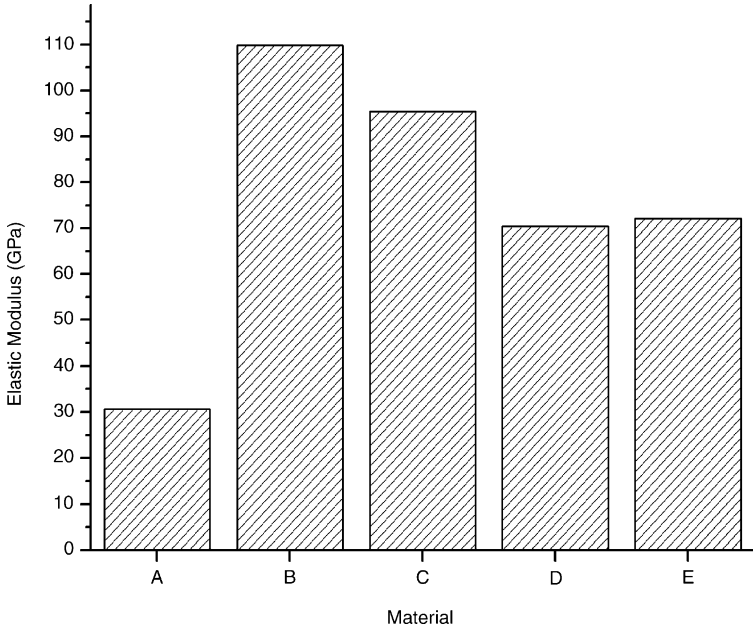

Fig. 18. Elastic moduli of coatings, bulk glass and stoneware. (A) As-sprayed coating (4 p.b.), (B) 10–30 coating (4 p.b.), (C) bulk CZS glass (elastic waves), (D) stoneware (elastic waves), (E) stoneware (4 p.b.).

face are strong enough not to be broken or spalled (thanks to the coating excellent cohesion, excellent interface adhesion, and the good mechanical properties of crystalline phases).

Chemical resistance tests do not produce any visible effect without dye treatment. However, dye treatment indicates a certain susceptibility to acid attack, as the attacked area is slightly stained: SEM micrographs (Fig. 17) reveal a selective attack on wollastonite: areas where wollastonite prevails have been dissolved in the solution causing an increase in superficial porosity. Indeed, in this system, ZrO_2 is the component mostly enhancing chemical resistance, therefore, the formation of a phase depleted in this element (wollastonite) lowers its chemical resistance. This is a trouble connected with the nature of the CZS system itself, not with the deposition or devetrification technique: spraying a different system would overcome it.

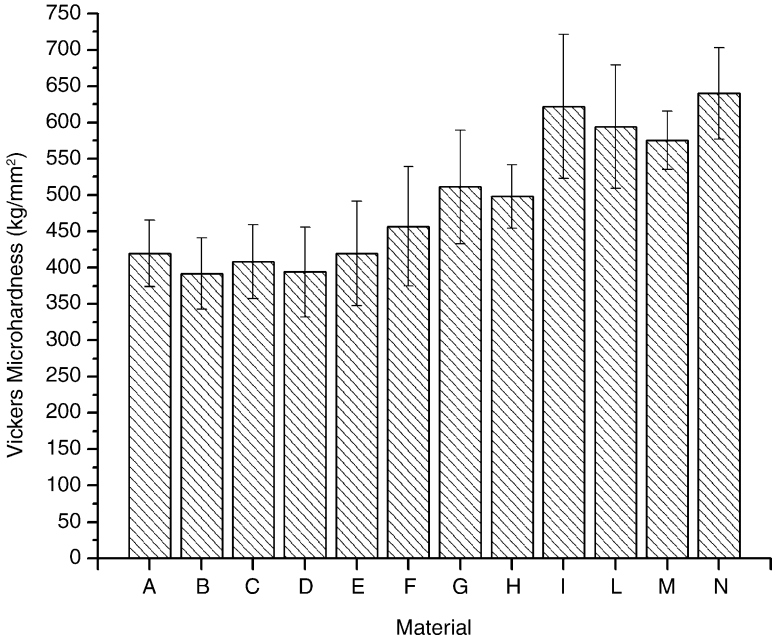

Fig. 19. Vickers microhardness (load in gram indicated in parenthesis, time = 15 s). (A) Stoneware (25), (B) CAS glaze 1130 °C 40′ (25), (C) CAS glaze 1200 °C 45′ (25), (D) CZS glaze 1130 °C 40′ (25), (E) CZS glaze 1200 °C 45′ (25), (F) as-sprayed coating (25), (G) 9–30 coating (25), (H) 9–60 coating (25), (I) 10–30 coating (50), (L) 10–15 coating (50), (M) bulk CZS glass (25), (N) bulk CZS glass-ceramic (50).

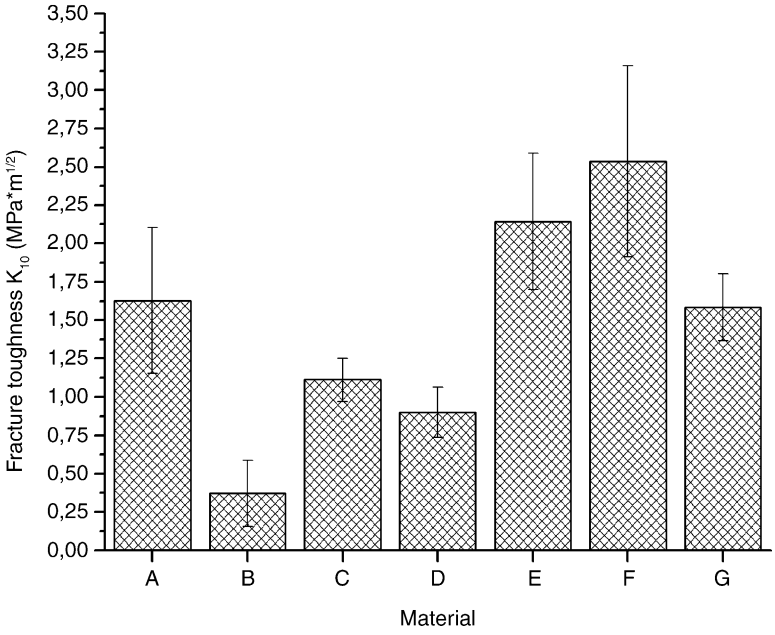

Fig. 20. Fracture toughness for stoneware, coatings and bulk glass. (A) Stoneware (P = 500 g), (B) as-sprayed coating (P = 100 g), (C) 9–30 coating (P = 300 g), (D) 9–60 coating (P = 300 g), (E) 10–30 coating (P = 500 g), (F) 10–15 coating (P = 500 g), (G) bulk CZS glass (P = 300 g).

4. Mechanical properties

4.1. Elastic modulus

The elastic modules are listed in Fig. 18. It can be noticed that the elastic modulus of as-sprayed coatings is about 30% of that of bulk CZS glass, which represents the maximum possible cohesion for the coating material (30.62 GPa against 95.35 GPa). It has been reported[12,21] that plasma-sprayed coatings have elastic modules which are significantly lower than those of corresponding bulk materials because pores and microcracks reduce cohesion and, in particular, splat interfaces start giving up when loaded, and that such behaviour becomes particularly significant in bending tests (3- or 4-points, as in this case); since various defects were actually detected in as-sprayed coatings, this result is well-explained by these observations. The 10–30 thermal treatment allows sintering and induces an almost complete crystallization: sintering greatly enhances cohesion, so that the material tends to be more stiff and linear in its deformation. Furthermore, crystals being more orderly and (generally) more close-packed atomic structures than glass networks, their formation implies the transition to a more intrinsically stiff structure. For this reason, the coating elastic modulus exceeds that of bulk CZS glass (109.85 GPa): this indicates that treatments at 1050 °C raise the coating mechanical properties almost up to their potential maximum. The elastic modulus of crystallized bulk CZS glass-ceramic could not be measured because, even after several hours of heat treatment at 1050 °C, the crystallization of the bulk material is only superficial.

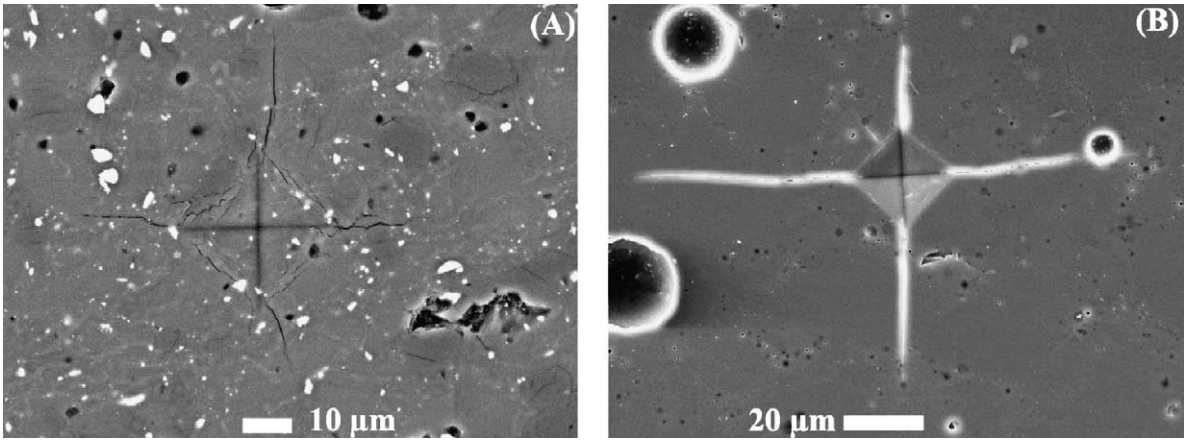

Fig. 21. Cracked Vickers microindents for fracture toughness determination on polished surface of porcelanized stoneware (A) and of 9–60 coating (B).

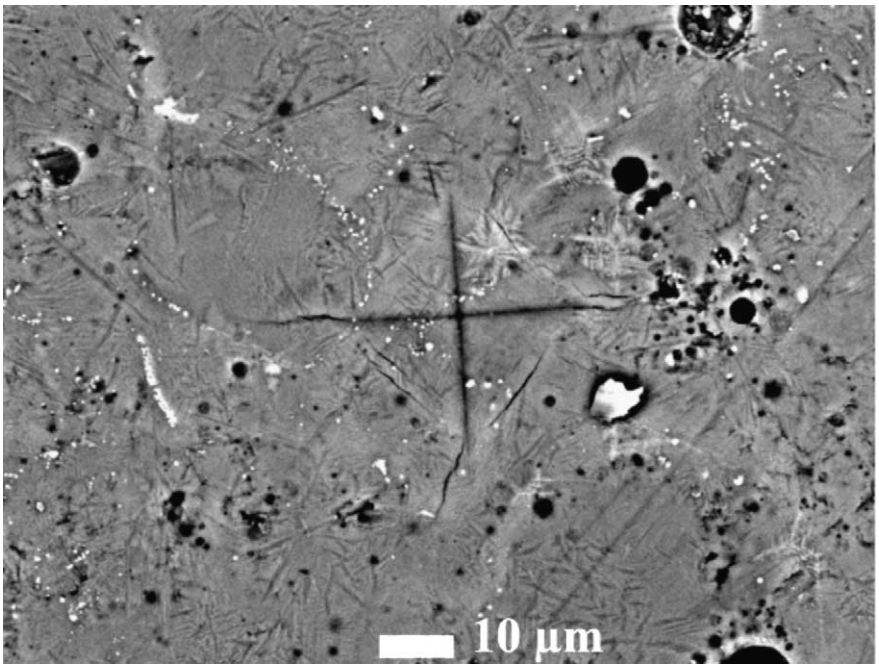

Fig. 22. Cracked Vickers microindent for fracture toughness determination on polished surface of 10–15 coating.

Stoneware elastic modulus is almost the same when measured with both techniques, their comparability is thus assessed.

4.2. Vickers microhardness

Fig. 19 indicates Vickers microhardness for different materials. The coatings do not show significant differences between surface and cross-sectional hardness, therefore only the latter has been reported. The liability of a material to local plastic deformation depends first of all on its structure (packing of atoms, strength of interatomic bonds), but also on its microstructure, because, in a material which does not have an ideal cohesion, weak links can collapse and cause a higher deformation. The influence of the material structure is clear when comparing the hardness of stoneware and of as-sprayed coatings: although stoneware has a much more compact microstructure, it possesses lower hardness due to the structural properties of the phases that are present. However, a clear hardness increase dependent on microstructure is

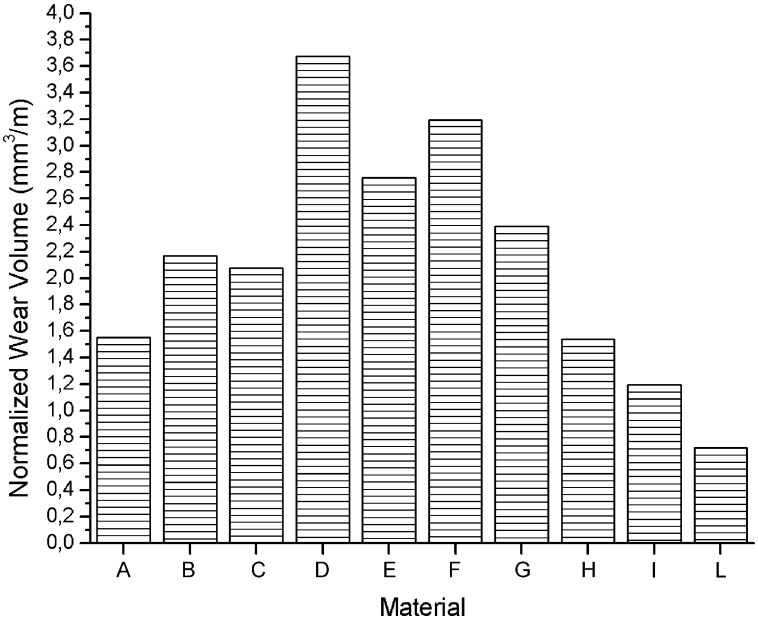

Fig. 23. Normalized wear volume for the tested materials. (A) Stoneware, (B) CAS glaze 1130 °C 40′, (C) CAS glaze 1200 °C 45′, (D) CZS glaze 1130 °C 40′, (E) CZS glaze 1200 °C 45′, (F) as-sprayed coating, (G) 9–30 coating, (H) 9–60 coating, (I) 10–30 coating, (L) 10–15 coating.

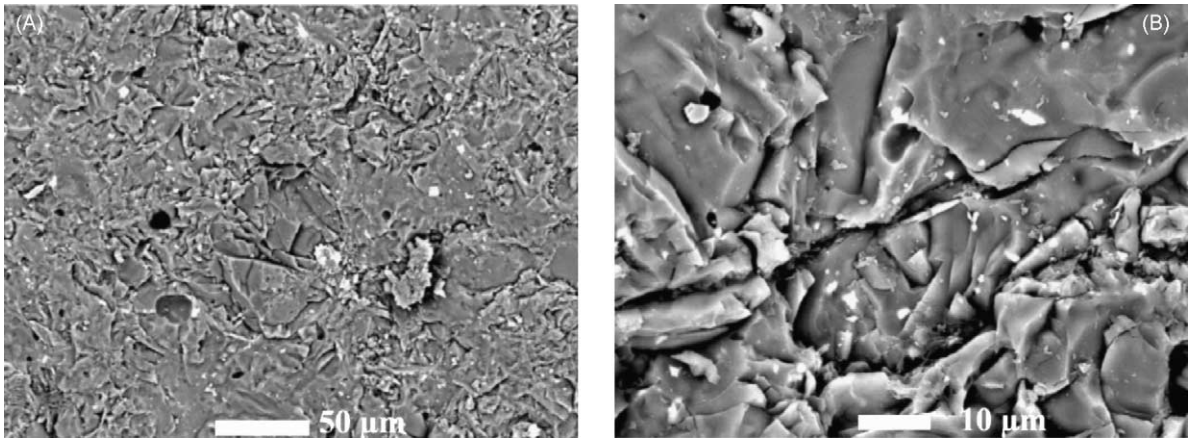

Fig. 24. SEM micrographs of stoneware abrasion trace at different magnifications: (A) 400×, (B) 1600×. (B) A crack going round a quartz grain.

noticeable passing from as-sprayed coating, to 9–30 and 9–60 coatings, and to bulk CZS glass. Therefore, when considering materials of the same kind, Vickers microhardness is a reliable indication of the microstructural cohesion,[28] just like elastic modulus. As already mentioned, crystals are generally more orderly and compact structures than glasses of similar composition, therefore the coating crystallization causes a further hardness increase because the structural change effect is added to good microstructural cohesion: 10–30 and 10–15 coating hardness exceeds that of bulk CZS glass, as in the case of the elastic modulus, and is substantially equal to that measured on the crystallized surface of annealed CZS glass-ceramic. As observed in the case of elastic modulus, these treatments maximize the coating properties. The small microstructural difference noticed in part 1 between 10–15 and 10–30 coatings reflects in a slight hardness difference between them.

4.3. Fracture toughness

Fracture toughness is more dependent on microstructure and less on structure than microhardness, because microstructural features can significantly affect stresses distributions in a material and hence alter crack formation and propagation. Therefore, it is easier to justify the comparison of fracture toughness between different materials with micrographic observations: a material with many pores and defects will thus be less tough than a compact material, and the presence of reinforcing phases will further raise toughness. With these simple considerations, results reported in Fig. 20 are easily explained. Stoneware is quite compact, with small pores and no cracks, and it is reinforced by the presence of crystalline phases like quartz and, especially, mullite. Therefore, it is much tougher than as-sprayed CZS coatings, where the numerous microstructural defects become stress intensifiers and favour crack formation and constitute a preferential path for its propagation. It is also tougher than 9–30 and 9–60 treated coatings, because, even though the defectiveness of these coatings is comparable to or lower than stoneware, they are substantially glassy, with no reinforcing phases, so that crack propagation is not hindered: in stoneware, instead, cracks are forced to move around the more tough crystalline phases, with greater energy consumption. These coatings are less tough than bulk glass, since this latter contains no

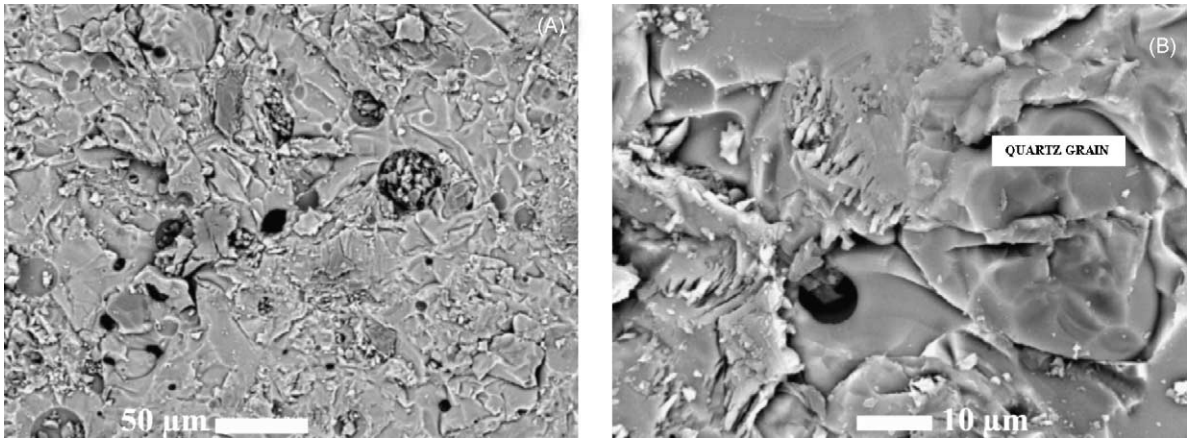

Fig. 25. SEM micrographs of CAS—1200 °C 45′ glaze at different magnifications: (A) 400×, (B) 1600×.

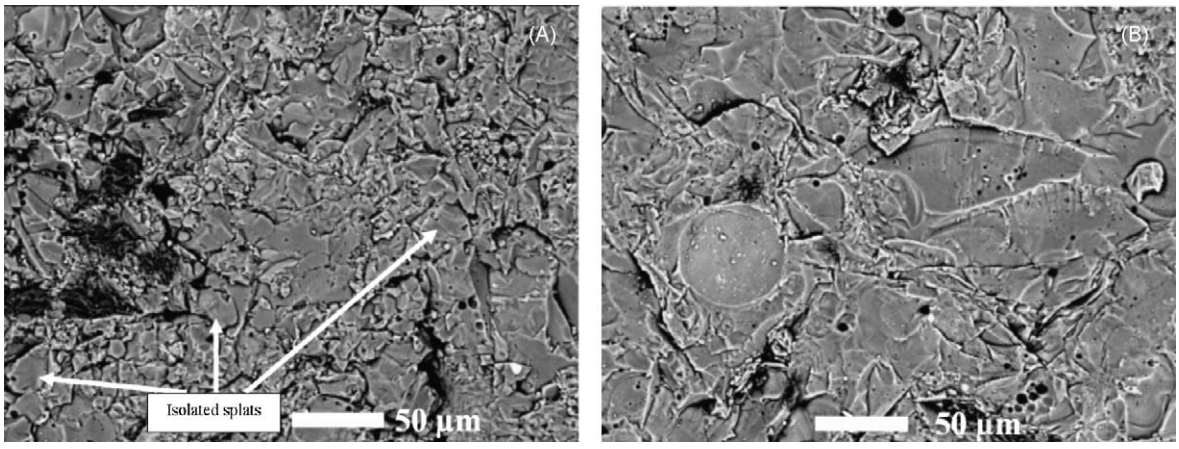

Fig. 26. Abrasion trace micrograph in as-sprayed CZS coating, showing fragile splats detachment (A); abrasion trace micrograph of 9–30 coating (B).

porosity. Stoneware is instead less tough than 10–30 and 10–15 treated coatings, where the numerous, interlaced wollastonite crystals deflect cracks very frequently, and further reinforcing is due to the presence of very small $Ca_2ZrSi_4O_{12}$ grains. Furthermore, in stoneware there are some glassy regions with no crystals, and the quartz grains, having been introduced as a raw material (not formed during firing) and undergoing a phase transition with significant volume change, might sometimes have low cohesion with the matrix. As observed in part 1, 10–15 coating has smaller and more numerous grains: this implies more crack deflections and, therefore, higher toughness, as experimentally measured. Micrographs of cracked Vickers microindentations employed in fracture toughness measurement on porcelanized stoneware and 9–60 coating are shown in Fig. 21A and B, a cracked indentation on 10–15 coating is shown in Fig. 22.

4.4. Deep abrasion resistance

Fig. 23 indicates the deep abrasion resistance for all tested coatings, glazes and stoneware. First of all, it can be noticed that stoneware is more resistant than the CAS glaze, one of the best industrial glazes currently in production: this confirms that the limits imposed by traditional technologies on glazing materials seriously prejudices glazes properties. The morphology of the stoneware abrasion trace, observed through SEM micrographs (Fig. 24A), is quite irregular, with superficial and sub-superficial cracks which appear to have undergone several deflections. This indicates that, as predictable, brittle fracture is the most important abrasion mechanism: the pressure of abrasive grains against the surface of the material cause a stress peak at a depth of a few micrometers, which originates cracks propagating themselves up to the surface,

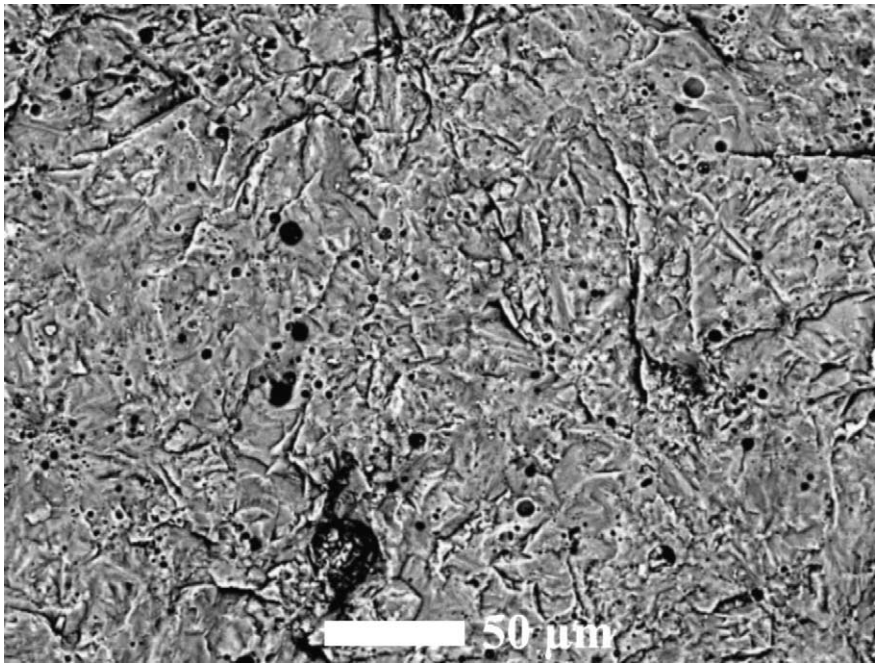

Fig. 27. Abrasion trace micrograph of 10–15 coating at low magnification, 400×.

with subsequent material removal. The frequent crack deflections are caused by the presence of crystalline phases (Fig. 24B) shows a crack forced to move round a quartz grain, and confirm their toughening effect, discussed in the previous section: this is consistent with toughness measurements. It must also be noticed that some plastic ploughing is present: ceramics can undergo local plastic deformation on a micrometric scale, and this happens in this case because the employed abrasive (corundum) is significantly harder than stoneware.

In the CAS glaze, the toughening effect of the quartz grains observed in the first part is particularly clear (Fig. 25A and B): cracks are forced to go round them, with greater energy consumption due to the deflection. However, the detected presence of large pores compromises the glaze resistance; therefore, the glaze fired at 1130 °C, being more porous, has lower resistance. This is even more stressed in the CZS-based glazes, where the pores are larger than the corresponding CAS glazes. These results confirm that, as anticipated in the first part, traditional glazing technologies do not allow optimal exploitation of CZS system potentialities: the CZS-based glaze fired at 1130 °C for 40 min has the lowest abrasion resistance among all tested materials, because it contains a great amount of porosity and also phases with lower mechanical properties than the pure frit (albite). The markedly different abrasion resistances between materials with similar hardness (stoneware and glazes) confirm that, when abrasion mechanism is dominated by brittle fracture, hardness is not the most significant parameter.

As-sprayed CZS coating has quite low abrasion resistance: being slightly harder than stoneware, but definitely more brittle, it furthermore confirms the prevalent effect of fracture toughness on abrasion resistance. SEM micrographs clarify the cause of such low toughness and abrasion resistance (Fig. 26A): splats are easily fractured because of their glassy nature, and, most importantly, cracks preferentially propagate along splat boundaries, causing the removal of entire splats at a time from the coating. Splats with cracks propagating around them are clearly noticeable: it is therefore reasonable to assume that splats above have been completely detached from them.

The 9–30 and 9–60 coatings are tougher than as-sprayed coatings because of their higher cohesion, indicated also by the hardness increase, but they still remain more brittle than stoneware because they are substantially glassy. The micrographs (Fig. 26B) show plain fracture surfaces and cracks propagating straightforwardly, as a confirm to former comments on fracture toughness. Being harder but less tough than stoneware, their abrasion resistance is comparable to that of stoneware. Some plastic ploughing is also noticeable, because corundum abrasive grains are much harder than CZS glass.

The 10–30 and 10–15 samples possess high cohesion, and their microstructure is completely different from the previous coatings, being completely crystalline. This explains the higher abrasion resistance than stoneware: an almost 30% improvement is achieved with 10–30 treatment, and a 50% improvement follows the 10–15 treatment, which produces smaller and more numerous crystals and, therefore, more toughening. Abrasion trace micrographs (Figs. 27 and 28) on 10–15 show very irregular fracture surfaces, caused by continuous cracks deflections, even more frequent than in stoneware. Crack deflections are due to the presence of the interlaced wollastonite dendrites and the several small $Ca_2ZrSi_4O_{12}$ grains. Higher hardness than stoneware also

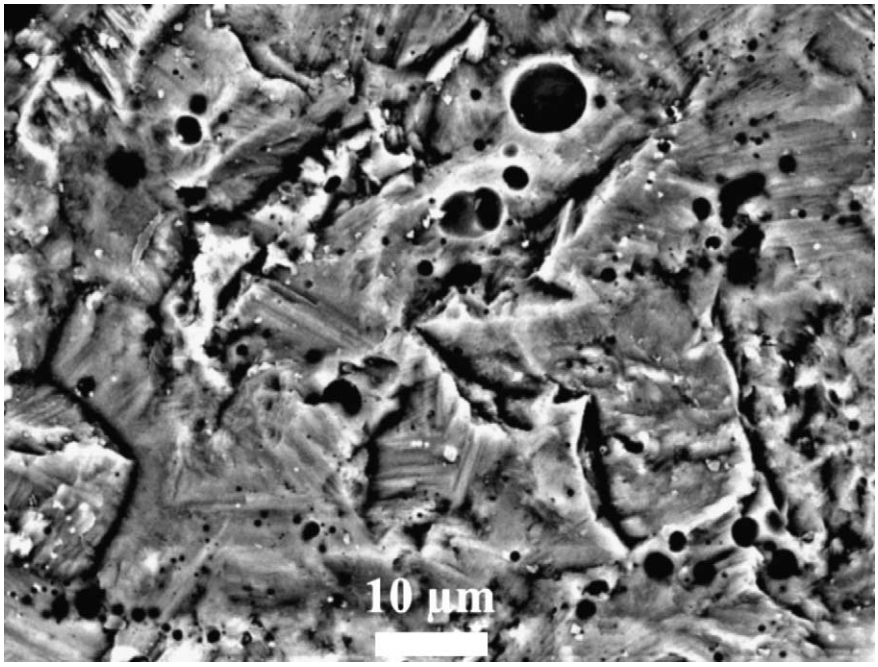

Fig. 28. Abrasion trace micrograph of 10–15 coating at high magnification, 1600×.

means lower tendency to local plastic deformation, in fact no significant ploughing has been detected in these coatings.

4.5. Adhesion strength

Sample break-up occurred in the substrate: coating adhesion and cohesion are therefore greater than substrate tensile strength, as could have been expected taking into consideration toughness measurements and 10–30 coatings microstructure. Tensile strength is about 2 MPa; therefore 10–30 coating adhesion and cohesion is larger than this value.

5. Conclusions

These results indicate the feasibility of plasma-spraying a high-melting point frit, like CZS, on traditional ceramics. They also confirm that such high performance glass systems cannot be suitably exploited by traditional deposition techniques, because, even after mixing with lower melting point glass frits, they still do not sinter properly. Plasma-spraying, instead, enables pure highly performant coating materials to be deposited without substrate overheating. Moreover, removal of residual porosity is easier than powders sintering, as the starting point is an already quite compact system: lower densification treatment temperatures are suitable, thus preventing plastic deformation of the tile. Lower porosity than industrial glazes has been obtained in thermally treated coatings. Furthermore, a complete bulk devetrification can be induced in these systems through thermal treatment: the defects caused by the spraying process itself act as nucleating agents, promoting crystallization. Grain number and size are controllable, within a certain limit, by suitably choosing thermal treatment, in order to set the best conditions to enhance mechanical properties. Chemical resistance properties are not so controllable, since they mostly depend on the particular system composition; therefore, the glass-ceramic system choice is the only way to get significant enhancements.

The as-sprayed coatings have the typical microstructure and properties of plasma-sprayed coatings: pores, intersplat and intrasplat cracks reduce cohesion and, hence, elastic modulus and hardness compared to the bulk material; furthermore, splat boundaries constitute a preferential cracking path, thus reducing toughness. For this reason, porosity removal and controlled crystallization through a proper post-process thermal treatment are needed to enhance mechanical properties: the optimal thermal treatment consists in an isotherm at 850 °C for 30′ and a second isotherm at 1050 °C for 15′. The above results show that, to attain optimal abrasion resistance, cohesion improvement only is not enough, but toughening mechanisms must be introduced. Therefore, both sintering and crystallization of the coating are key requirements in the thermal treatment definition: as long as the coating is glassy, even if great sintering is achieved, the abrasion resistance of stoneware is not overcome, whereas, when crystallization is induced, a definite increase in all mechanical properties is obtained and the abrasion resistance exceeds that of stoneware.

Mechanical characterization indicates that both hardness and elastic modulus are good cohesion indicators when materials of the same kind are considered. However, abrasion resistance mostly depends on fracture toughness, since abrasion in ceramics and glasses is mainly due to brittle fracture, not to plastic deformation (even though plastic deformation is possible in these materials on a micrometric scale). Moreover, hardness also depends significantly on materials structure, whereas crack propagation is a primarily microstructural phenomenon; therefore, fracture toughness, which is more insensitive of materials structure and more dependent on their microstructure, better correlates to abrasion resistance.

Interface adhesion appears to be good even in as-sprayed coatings. Thermal treatments greatly enhance it, not only because mechanical interlocking is promoted by viscous flow, but also through crystals growth from the substrate interface into the coating: the adhesion mechanism, from merely mechanical, becomes also chemical.

Acknowledgements

The authors are grateful to M.I.U.R. for the financial support; to Centro Sviluppo Materiali S.p.A. (Castel Romano, Italy) Surface Engineering Unit, in particular to Ing. Fabrizio Casadei and Mr. Edoardo Severini, for the spray runs; to Colorobbia S.p.A. for the frits supplying and the realization of the glazed tiles and to Marazzi S.p.A. for the tiles supplying.

References

1. Emiliani, G. P. and Corbara, F. *Tecnologia Ceramica—Volume II: La Lavorazione*. Gruppo Editoriale Faenza Editrice, Faenza, 1999, pp. 383–441.
2. Herman, H., Sampath, S. and McCune, R., Thermal spray: current status and future trends. In *Thermal Spray Processing of Materials*, ed. S. Sampath and R. McCune. *MRS Bull.*, July 2000, 17–25.
3. Vardelle, A., Fauchais, P., Dussoubs, B. and Themelis, N. J., Heat generation and particle injection in a thermal plasma torch. *Plasma Chem. Plasma Process.*, 1998, **18**, 551–572.
4. Matejicek, J., Sampath, S., Gilmore, D. and Neiser, R., In situ measurement of residual stresses and elastic moduli in thermal sprayed coatings. Part 2: processing effects on properties of mo coatings. *Acta Materialia* 2003, **51**, 873–885.
5. Bianchi, L., Denoirjean, A., Blein, F. and Fauchais, P., Microstructural investigation of plasma-sprayed ceramic splats. *Thin Solid Films*, 1997, **299**, 125–135.
6. Ahmaniemi, S., Tuominen, J., Vuoristo, P. and Mäntylä, T., Sealing procedures for thick thermal barrier coatings. *J. Thermal Spray Technol.*, 2002, **11**, 320–331.
7. Ang, C. B., Devasenapathi, A., Ng, H. W., Yu, S. C. M. and Lam, Y. C., A proposed process control chart for dc plasma spraying process. part ii. experimental verification for spraying alumina. *Plasma Chem. Plasma Process.*, 2001, **21**, 401–419.
8. Hawthorne, H. M., Erickson, L. C., Ross, D., Tai, H. and Troczynski, T., The microstructural dependence of wear and indentation

behaviour of some plasma-sprayed alumina coatings. *Wear*, 1997, **203/204**, 709–714.
9. Westergärd, R., Erickson, L. C., Axén, N., Hawthorne, H. M. and Hogmark, S., The erosion and abrasion characteristics of alumina coatings plasma sprayed under different spraying conditions. *Tribol. Int.*, 1998, **31**, 271–279.
10. Erickson, L. C., Hawthorne, H. M. and Troczynski, T., Correlations between microstructural parameters, micromechanical properties and wear resistance of plasma sprayed ceramic coatings. *Wear*, 2001, **250**, 569–575.
11. Z. Strnad, *Glass-Ceramic Materials*. Elsevier, New York, 1986, pp. 166–184.
12. Wang, Z., Kulkarni, A., Deshpande, S., Nakamura, T. and Herman, H., Effect of pores and interfaces on effective properties of plasma sprayed zirconia coatings. *Acta Materialia*, 2003, **51**, 5319–5334.
13. Schrooten, J. and Helsen, J. A., Adhesion of bioactive glass coating to Ti6Al4V oral implant. *Biomaterials*, 2000, **21**, 1461–1469.
14. Gabbi, C., Cacchioni, A., Locardi, B. and Guadagnino, E., Bioactive glass coating: physicochemical aspects and biological findings. *Biomaterials*, 1995, **18**, 515–520.
15. Bessmertnyi, V. S., Min'ko, N. I., Dyumina, P. S. and Dridzhd, N. A., Evaluation of the competitiveness of household glassware decorated by plasma spraying. *Glass Ceram.*, 2002, **59**, 251–254.
16. Bessmertnyi, V. S., Krokhin, V. P., Panasenko, V. A., Drizhd, N. A., Dyumina, P. S. and Kolchina, O. M., Plasma rod decorating of household glass. *Glass Ceram.*, 2001, **58**, 214–215.
17. Gawne, D. T., Qiu, Z., Bao, Y., Zhang, T. and Zhang, K., Abrasive wear resistance of plasma-sprayed glass-composite coatings. *J. Thermal Spray Technol.*, 2001, **10**(4), 599–603.
18. Weaver, D. T., Van Aken, D. C. and Smith, J. D., The role of bulk nucleation in the formation of crystalline cordierite coatings produced by air plasma spraying. *Mater. Sci. Eng.*, 2003, **A339**, 96–102.
19. Loreto, A., Lusvarghi, L., Bartuli, C., Manfredini, T., Tempesta, G. and Bolelli, G., Production and Characterization of Plasma-Sprayed Glass and Glass-Ceramic Coatings. To be presented in 7th AIMAT Congress, Ancona, Italy, 22–24 June 2004.
20. Siligardi, C., D'Arrigo, M. C. and Leonelli, C., Sintering criteria for glass-ceramic frits belonging to the $CaO–ZrO_2–SiO_2$ system. *Am. Ceram. Soc. Bull.*, 2000, **79**, 88–92.
21. Kim, H.-J. and Kweon, Y.-G., Elastic modulus of plasma-sprayed coatings determined by indentation and bend tests. *Thin Solid Films*, 1999, **342**, 201–206.
22. Gosh, S., Das, S., Bandyopadhyay, T. K., Bandyopadhyay, P. P. and Chattopadhyay, A. B., Indentation responses of plasma-sprayed ceramic coatings. *J. Mater. Sci.*, 2003, **38**, 1565–1572.
23. Ponton, C. B. and Rawlings, R. D., Vickers indentation fracture toughness test. Part 1: review of literature and formulation of standardised indentation toughness equations. *Mater. Sci. Technol.*, 1989, **5**, 865–872.
24. Ponton, C. B. and Rawlings, R. D., Vickers indentation fracture toughness test. Part 2: appication and critical evaluation of standardised indentation toughness equations. *Mater. Sci. Technol.*, 1989, **5**, 961–976.
25. Fukumoto, M., Nishioka, E. and Nishiyama, T., New criterion for splashing in flattening of thermal sprayed particles onto flat substrate surface. *Surf. Coat. Technol.*, 2002, **161**, 103–110.
26. Zhang, H., Wang, X. Y., Zheng, L. L. and Jiang, X. Y., Studies of splat morphology and rapid solidification during thermal spraying. *Int. J. Heat Mass Transfer*, 2001, **44**, 4579–4592.
27. Mostaghimi, J., Pasandideh-Fard, M. and Chandra, S., Dynamics of splat formation. *Plasma Chem. Plasma Process.*, 2002, **22**, 61–83.
28. *ASM Handbook: Volume 8: Mechanical Testing and Evaluation*, ed. H. Kuhn and D Medlin. ASM International, Materials Park, Ohio, USA, 2000, p. 248.